

Acoustoelasticity in soft solids: Assessment of the nonlinear shear modulus with the acoustic radiation force

J.-L. Gennisson,^{a)} M. Rénier, S. Catheline, C. Barrière, J. Bercoff, M. Tanter, and M. Fink
*Laboratoire Ondes et Acoustique, ESPCI, CNRS UMR 7587, INSERM, Université Paris VII,
10 rue Vauquelin, 75231 Paris cedex 05, France*

(Received 4 July 2007; revised 28 August 2007; accepted 29 August 2007)

The assessment of viscoelastic properties of soft tissues is enjoying a growing interest in the field of medical imaging as pathologies are often correlated with a local change of stiffness. To date, advanced techniques in that field have been concentrating on the estimation of the second order elastic modulus (μ). In this paper, the nonlinear behavior of quasi-incompressible soft solids is investigated using the supersonic shear imaging technique based on the remote generation of polarized plane shear waves in tissues induced by the acoustic radiation force. Applying a theoretical approach of the strain energy in soft solid [Hamilton *et al.*, *J. Acoust. Soc. Am.* **116**, 41–44 (2004)], it is shown that the well-known acoustoelasticity experiment allowing the recovery of higher order elastic moduli can be greatly simplified. Experimentally, it requires measurements of the local speed of polarized plane shear waves in a statically and uniaxially stressed isotropic medium. These shear wave speed estimates are obtained by imaging the shear wave propagation in soft media with an ultrafast echographic scanner. In this situation, the uniaxial static stress induces anisotropy due to the nonlinear effects and results in a change of shear wave speed. Then the third order elastic modulus (A) is measured in agar-gelatin-based phantoms and polyvinyl alcohol based phantoms. © 2007 Acoustical Society of America. [DOI: 10.1121/1.2793605]

PACS number(s): 43.25.Dc, 43.25.Ed [OAS]

Pages: 3211–3219

I. INTRODUCTION

For almost two decades, the study of shear wave propagation in soft media became of a peculiar interest in the ultrasonic medical imaging community, especially in the field of dynamic elastography.^{1–3} Methods such as sonoelastography^{4,5} or transient elastography^{6,7} have shown their efficiency to determine the elastic properties of biological soft tissues. However, to date, advanced techniques in that field have been concentrated on the estimation of the second order elastic modulus (μ). In order to better understand pathologies, new refinements were developed to study other mechanical parameters such as anisotropy,⁸ viscoelasticity,^{9,10} or nonlinearity.¹¹ Transient elastography is one of the most efficient approaches, as it images in real time the transient propagation of shear waves in soft media using ultrafast echographic scanners. Based on this concept, three possible ways to quantify nonlinearity in soft solids: Propagation of shocked shear waves,¹² nonlinear interaction between shear waves¹³ and acoustoelasticity.¹¹

The acoustoelasticity theory in solids has been first established by Hugues and Kelly in 1953¹⁴ using the second order and third order elastic coefficient. These parameters come from the expansion of the strain energy density as a function of the invariants of the strain tensor in “Lagrangian” coordinates.¹⁵ The third order moduli can also be expressed as a function of the Landau coefficients (A , B , C).¹⁶ Experimentally, acoustoelasticity consists of measuring the speed of acoustic waves in stressed solids. The third order moduli are

deduced from the slope of the ultrasonic waves velocities as a function of the uniaxial stress or of the hydrostatic pressure applied to the sample. However, acoustoelastic analysis has usually been applied to compressible engineering materials. From our knowledge, regarding soft solids, biological tissues or “nearly” incompressible materials, only few works have been developed on the acoustoelasticity theory for hyperelastic media^{17,18} or on the nonlinear properties of tissue-like phantoms.¹⁹

In a recent paper, shear wave propagation theory in soft solids brought new ideas in the field of elasticity theory. Hamilton *et al.*²⁰ suggested a new expression of the elastic energy density. Applied to nonlinear shear wave experiments reported in Ref. 12, Zabolotskaya *et al.*²¹ obtained a straightforward nonlinear equation where only three elastic coefficients are involved. In this paper, this approach is applied to the field of acoustoelasticity. It results in evolution equations for shear waves in stressed incompressible media that depend on only two elastic coefficients.

In a previous paper,¹¹ we proposed the estimation of the shear wave speed in a medium submitted to an uniaxial stress, using the one dimensional (1D) transient elastography technique.⁸ In these soft solid acoustoelasticity experiments, there were two main difficulties. First, it was difficult to obtain a uniform and constant uniaxial stress, as the stress field in the samples was highly dependent on the boundary conditions. The experimental setup has been improved by using a cylindrical phantom and a mechanical guide to insure a vertical direction of the applied loads. Second, in the 1D transient elastography approach, cylindrical shear waves were generated by giving a low frequency pulse (~ 100 Hz) at the surface of the phantom with a point source

^{a)}Electronic mail: jl.gennisson@espci.fr

(the transducer itself). Thus, in the near field coupling between longitudinal waves and shear waves were nonnegligible. Moreover, model equations were established for plane waves, so experimental assessments were biased by strong diffraction effects. Consequently the experimental set-up has been enhanced by replacing the mechanical vibrator by the acoustic radiation force technique as a shear wave source.²² This technique enables the controlled generation of quasi-plane shear waves in the medium by focusing an ultrasound beam successively at several depths in the medium thus generating several in-depth sources of shear waves. The electronic steering of the ultrasonic beam permits to move the shear source at a higher speed than resulting shear waves propagation speed leading to a supersonic regime. Thus, contrary to the 1D transient elastography, shear diffraction effects were strongly minimized and interaction between longitudinal waves and shear deformations were excluded.

In this paper, the theoretical background of the acoustoelasticity technique is introduced in the first section to deduce the nonlinear shear coefficient A of soft solids. Theoretical equations derived in this section are compared with the classical approach in solids. In the next section, the experimental setup and experimental results are described. Two soft materials used as phantoms in medical imaging are tested: agar-gelatin (AG) phantoms and polyvinyl alcohol cryogel (PVA) phantoms. Finally, the experimental assessments of the nonlinear shear coefficient are discussed.

II. THEORETICAL BACKGROUND

The general principle of acoustoelasticity is based on the expressions of the speed of elastic waves in a uniaxially stressed lossless solid. Basic equations are summarized as follows. In “Lagrangian” coordinates (\mathbf{a}, t) (\mathbf{a} is the equilibrium position of the particle, t is the time), equations of motion are

$$\rho_0 \ddot{u}_i = \frac{\partial P_{ik}}{\partial a_k} \quad \text{for } 1 \leq i, \quad k \leq 3. \quad (1)$$

where ρ_0 , P_{ik} , and $\ddot{\mathbf{u}} = \partial^2 \vec{\mathbf{u}} / \partial t^2$ designate the density, the Piola–Kirchhoff stress tensor (assuming Einstein summation convention of repeated indices) and the particle acceleration (second time derivative of the displacement \mathbf{u}), respectively. The Piola–Kirchhoff stress tensor is given in Lagrangian coordinates by²³

$$P_{ik} = \frac{\partial e}{\partial \left(\frac{\partial u_i}{\partial a_k} \right)}. \quad (2)$$

where e designates the strain energy density which can be developed up to the third order:

$$e = \mu I_2 + \frac{\lambda}{2} I_1^2 + \frac{A}{3} I_3 + B I_1 I_2 + C I_1^3. \quad (3)$$

where (μ, λ) are Lamé coefficients involved in the linear behavior of the solid and (A, B, C) are third order elastic coefficients of Landau, describing the quadratic nonlinear response of the deformed solid. (I_1, I_2, I_3) are invariants of the

Lagrangian strain tensor defined by Landau and Lifshitz.²³

Now let us consider the medium as incompressible. In such a media, an alternative expansion of the strain energy that permit separation of effects due to compressibility and shear deformation was recently defined by Hamilton *et al.*²⁰ and Zabolotskaya *et al.*²¹ Rather than express the strain energy in terms of invariants I_1, I_2 and I_3 as in Eq. (3), one choose instead to express the strain energy in terms of the set of independent invariants III_c, I_2 , and I_3 , where $III_c = \rho_0^2 / \rho^2$ is the third principal invariant of the Green deformation tensor. Thus here in incompressible media, $III_c = 1$, and the strain energy is

$$e = \mu I_2 + \frac{A}{3} I_3 + D I_2^2, \quad (4)$$

where D is the fourth order elastic constant. In the following sections, only propagation of plane waves of small amplitude will be considered, so fourth order terms will be neglected. Developing the invariants using the strain tensor \bar{S} defined by

$$S_{ik} = \frac{1}{2} \left(\frac{\partial u_i}{\partial a_k} + \frac{\partial u_k}{\partial a_i} + \frac{\partial u_l}{\partial a_i} \frac{\partial u_l}{\partial a_k} \right), \quad (5)$$

and according to Eq. (1), one obtains the following expression of the equation of motion:

$$\begin{aligned} \rho_0 \frac{\partial^2 u_i}{\partial t^2} = \frac{\partial P_{ik}}{\partial a_k} = & \mu \left(\frac{\partial^2 u_i}{\partial a_k^2} + \frac{\partial^2 u_k}{\partial a_i \partial a_k} \right) + \left(\mu + \frac{A}{4} \right) \\ & \times \left(\frac{\partial^2 u_l}{\partial a_i \partial a_k} \frac{\partial u_l}{\partial a_k} + \frac{\partial u_l}{\partial a_i} \frac{\partial^2 u_l}{\partial a_k^2} + \frac{\partial^2 u_k}{\partial a_l \partial a_k} \frac{\partial u_l}{\partial a_i} \right. \\ & + \frac{\partial^2 u_l}{\partial a_k^2} \frac{\partial u_l}{\partial a_i} + 2 \frac{\partial u_k}{\partial a_l} \frac{\partial^2 u_l}{\partial a_k \partial a_i} \left. \right) + \frac{A}{4} \left(\frac{\partial^2 u_k}{\partial a_k \partial a_l} \frac{\partial u_l}{\partial a_i} \right. \\ & \left. + \frac{\partial u_k}{\partial a_l} \frac{\partial^2 u_l}{\partial a_k \partial a_i} \right). \end{aligned} \quad (6)$$

In order to simplify further analytical developments, let us consider now some important points. First, in an acoustoelasticity experiment, two main displacements are involved. The static displacement due to the uniaxial stress applied and the dynamic displacement due to the propagation of shear waves induced here by the acoustic radiation force of the ultrasonic “palpating” beam. Moreover, shear strains must be of small amplitude compared to the static deformation induced by the uniaxial stress σ , which is the case experimentally here as ultrasonic radiation force induces very small (micrometric) displacements. Thus, the displacement can be expressed as the sum of the static displacement (\vec{u}^S) induced by the uniaxial stress and of the dynamic displacement (\vec{u}^D) due to the shear wave propagation:

$$\vec{u}^{\text{TOT}} = \vec{u}^D + \vec{u}^S. \quad (7)$$

Neglecting the nonlinear propagation of the shear wave and static deformations of higher order (i.e., $i = 1, 2, 3$), the wave equation is written as

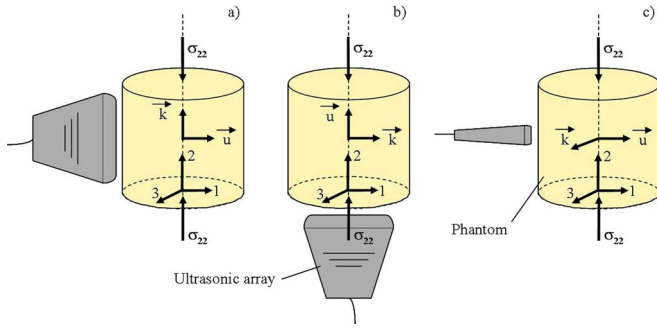


FIG. 1. (Color online) The three possible configurations generating (using the acoustic radiation pressure) and detecting (with an ultrafast scanner) the propagation of polarized shear waves in the phantom under uniaxial stress (σ_{22}). The three resulting shear waves are designated as (a) 12 or 32, (b) 21 or 23, and (c) 13 or 31.

$$\begin{aligned} \rho_0 \frac{\partial^2 u_i^D}{\partial t^2} = & \mu \left(\frac{\partial^2 u_i^D}{\partial a_k^2} + \frac{\partial^2 u_k^D}{\partial a_i \partial a_k} \right) + \left(\mu + \frac{A}{4} \right) \left(\frac{\partial^2 u_1^D}{\partial a_1 \partial a_k} \frac{\partial u_1^S}{\partial a_k} \right. \\ & + \frac{\partial u_1^S}{\partial a_i} \frac{\partial^2 u_1^D}{\partial a_k^2} + \frac{\partial^2 u_k^D}{\partial a_1 \partial a_k} \frac{\partial u_1^S}{\partial a_1} + \frac{\partial^2 u_1^D}{\partial a_k^2} \frac{\partial u_1^S}{\partial a_1} \\ & + 2 \frac{\partial u_k^S}{\partial a_1} \frac{\partial^2 u_i^D}{\partial a_k \partial a_1} \left. \right) + \frac{A}{4} \left(\frac{\partial^2 u_k^D}{\partial a_k \partial a_1} \frac{\partial u_1^S}{\partial a_i} \right. \\ & \left. + \frac{\partial u_k^S}{\partial a_1} \frac{\partial^2 u_1^D}{\partial a_k \partial a_i} \right). \end{aligned} \quad (8)$$

Second, for easier understanding and to simplify the calculations, one can deal with linearly polarized plane shear waves. For example, a plane wave that propagates along a_2 axis is considered, with a particle motion restricted to a_1 axis, according to those plotted on Fig. 1(a). The particle displacement in the wave is then expressed as $u_1^D(a_2, t)$. For sake of simplicity, the plane shear wave is characterized by the two indices according to the following convention 12. The first index corresponds to the direction of the shear displacement induced by radiation force (direction of polarization of the shear wave) and the second index corresponds to the axis of propagation of the shear wave. Let us chose the uniaxial stress directed along the a_2 axis. Then it comes:

$$\rho_0 \frac{\partial^2 u_1^D}{\partial t^2} = \mu \frac{\partial^2 u_1^D}{\partial a_2^2} + \left(2\mu + \frac{A}{2} \right) \left(\frac{\partial^2 u_1^D}{\partial a_2^2} \right) \left(\frac{\partial u_1^S}{\partial a_1} + \frac{\partial u_2^S}{\partial a_2} \right). \quad (9)$$

Third, because of the static uniaxial stress applied, three states and their coordinates need to be distinguished: the natural state, \mathbf{a} , the initial state, \mathbf{x} and the current state, \mathbf{y} related to shear wave propagation. It is useful to express the acoustoelastic equations in the initial coordinates, which, because of the infinitesimal nature of \mathbf{u}^D coincide with the laboratory (Eulerian) coordinates. For simplicity, one supposes that the initial stress and strain are uniform and defined by the static displacement \mathbf{u}^S : $\mathbf{x} = \mathbf{a} + \mathbf{u}^S$. The dynamic displacement \mathbf{u}^D , due to wave propagation is defined by: $\mathbf{y} = \mathbf{x} + \mathbf{u}^D$. The equation of motion for \mathbf{u}^D comes from development around the initial state of Eqs. (1) and (2). Then with the change of variable, $\mathbf{a} \rightarrow \mathbf{x}$, by neglecting again the terms of higher order and by use of the chain rule, it comes in the general case:

$$\frac{\partial^2 u_i^D}{\partial a_k^2} \cong \frac{\partial^2 u_i^D}{\partial x_k^2} \left(1 + 2 \frac{\partial u_k^S}{\partial x_k} \right), \quad \frac{\partial^2 u_k^D}{\partial a_i \partial a_k} \cong \frac{\partial^2 u_k^D}{\partial x_i \partial x_k}. \quad (10)$$

So for the plane wave $u_1^D(a_2, t)$, the wave equation in the new coordinates system becomes:

$$\begin{aligned} \rho_0 \frac{\partial^2 u_1^D}{\partial t^2} = & \frac{\partial^2 u_1^D}{\partial x_2^2} \left[\mu + 2\mu \left(\frac{\partial u_1^S}{\partial x_1} + 2 \frac{\partial u_2^S}{\partial x_2} \right) \right. \\ & \left. + \frac{A}{2} \left(\frac{\partial u_1^S}{\partial x_1} + \frac{\partial u_2^S}{\partial x_2} \right) \right]. \end{aligned} \quad (11)$$

Finally by using the Hooke's law²⁴ and assuming an incompressible medium (Poisson's ratio $\nu=0.5$), the spatial derivatives of the static displacement are:

$$\frac{\partial u_2^S}{\partial x_2} = -\frac{\sigma_{22}}{E} \approx -\frac{\sigma_{22}}{3\mu}, \quad \frac{\partial u_1^S}{\partial x_1} = \frac{\partial u_3^S}{\partial x_3} = \frac{\nu \sigma_{22}}{E} \approx \frac{\sigma_{22}}{6\mu}, \quad (12)$$

where E is Young's modulus. As one deals with compression (opposite of the dilatation), a negative stress was considered. Then, the nonlinear elastodynamic equation is rewritten as

$$\rho_0 V_{S12}^2 = \mu - \sigma_{22} \left(1 + \frac{A}{12\mu} \right), \quad (13)$$

with V_S being the shear wave velocity.

According to the axis defined by Fig. 1, the result is the same for the couple of indices 32. Regarding the other possible couples of indices, two more nonlinear elastodynamic equations are obtained.

For indices 21 or 23 the shear wave velocity is then:

$$\rho_0 V_{S21}^2 = \mu - \sigma_{22} \left(\frac{A}{12\mu} \right), \quad (14)$$

and for indices 13 or 31:

$$\rho_0 V_{S13}^2 = \mu + \sigma_{22} \left(1 + \frac{A}{6\mu} \right). \quad (15)$$

Note that Eqs. (13)–(15), if the medium is unstressed ($\sigma_{22}=0$), correspond to the classical shear wave propagation equation in an isotropic media. Thus, the medium reveals an anisotropic behavior resulting from the nonlinear effects.^{11,25} Moreover, changing the stress in Eqs. (13)–(15) is equivalent to modifying the shear modulus (μ) according to a linear dependence with a linear slope defined by the shear modulus (μ) and the third order nonlinear coefficient (A).

With this approach, theory of acoustoelasticity in incompressible media developed in this section of the present paper is fully consistent with classical acoustoelasticity theories defined in classical solids. For example, one can take as a comparison the theoretical framework developed by Hughes and Kelly.¹⁴ Hughes and Kelly establish expressions for velocities of elastic waves in stressed solids using Murnaghan's theory¹⁵ of finite deformations and third order terms in the energy. These expressions can also be expressed as a function of the Landau coefficient¹⁶ for plane shear waves under uniaxial stress. Assuming the material incompressible, one can use following statements: $\lambda \gg \mu$ and $B = -K = -(\lambda + \frac{2}{3}\mu)$,²⁶ the equations derived from Hughes and Kelly lead to Eqs.

(13)–(15). Similarly, using the theoretical approach of Thurston and Brugger²⁷ and summarized by Norris in Ref. 16, Eqs. (13)–(15) can be retrieved.

Thus, the application of both previous theories (Hugues and Kelly;¹⁴ Thurston and Brugger²⁷) to incompressible media is consistent with Hamilton *et al.*²⁰ and Zabolotskaya *et al.*²¹ papers. With this theoretical approach, in the case of soft solids, the separation of compressibility and shear deformations is possible and shear velocities depend only on the second and third order shear elastic moduli (μ, A). The influence of second and third order elastic coefficients related to longitudinal waves can be neglected. Therefore, compared to expressions in isotropic and compressible medium,¹¹ neither the third order Landau coefficients B and C [Eq. (3)] (B is defined as the nonlinear coefficient of the coupling term between shear and longitudinal waves and C is defined as the nonlinear coefficient for longitudinal waves) nor λ the second Lamé coefficient (λ is linked to the compressibility of the material) have any effect on the determination of shear velocities.

In the following section, as the supersonic shear imaging technique enables the controlled generation of quasiplane shear waves and the total discrimination in time between shear and compressional deformations during the acquisition due to the huge discrepancy between shear ($\sim 1 \text{ m s}^{-1}$) and compressional wave ($\sim 1500 \text{ m s}^{-1}$) speeds; we will take advantage of these relationships [Eqs. (13)–(15)] to estimate the linear and nonlinear elastic moduli (μ, A) in an acoustoelasticity experiment.

III. MEASUREMENT SYSTEM

The experiments were performed on two kinds of quasi-incompressible soft solids commonly used for the mimicking of soft tissues: five AG phantoms and three PVA phantoms.

The five AG phantoms were prepared with different concentrations of gelatin and agar diluted in water (initially heated at $50 \text{ }^\circ\text{C}$) following a strict procedure earlier described in Ref. 28. Two AG phantoms (GEL_1 and GEL_4) were cylinders of 12.5 cm diameter and 15 cm high, with a concentration of 3% by weight of agar (Agar, Prolabo, Fontenay/Bois, France) and 5% and 15% by weight of gelatin (Gelatin, Prolabo, Fontenay/Bois, France), respectively. The three other ones (GEL_2, GEL_3, GEL_5) were cylinders of 12 cm diameter and 15 cm high with 3% by weight of agar and 7%, 10%, and 8.5% by weight of gelatin, respectively. The agar was used as scatterers and gelatin was used as matrix.

PVA phantoms were constituted of 10% by weight of PVA (polyvinyl alcohol hydrolyzed, Sigma-Aldrich, St Louis, MO) dissolved in water. The solution container was heated in hot water to $80 \text{ }^\circ\text{C}$, and to minimize dehydration the container was covered. 3% by weight of Sigmacell (Sigmacell Cellulose type 20, Sigma-Aldrich, St Louis, MO) was added to serve as scatterers. The three PVA phantoms were cylinders of a 15 cm high and 12 cm diameter. PVA phantoms underwent two (PVA_1), three (PVA_2) and five (PVA_3) freezing–thawing cycle to polymerize them with a certain level of elasticity as described in previous papers.^{29,30}

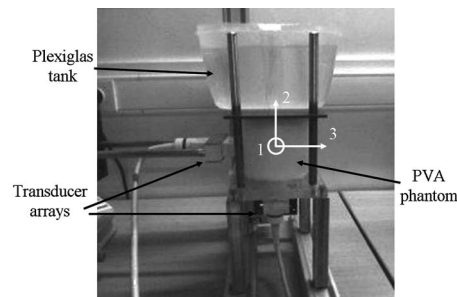


FIG. 2. Experimental set-up on a PVA phantom (PVA_2). Two transducer arrays are placed along the vertical axis of the phantom and at the bottom of the phantom, in order to measure the shear waves propagation with the 21 or 23 [Eq. (19)] and the 12 or 32 [Eq. (18)] indices respectively. During this experiment, the tank was incrementally filled with water in steps of 0.3 kg.

In experiments, a rigid Plexiglas tank was added on top of the phantoms and filled with different amounts of water [e.g., with the agar-gelatin phantom GEL_4, from 0.3 kg (weight of the Plexiglas plate and tank) to about 2.1 kg in incremental steps of 0.3 kg step] to control the uniaxial stress (Fig. 2). The loading charges were adapted depending of the phantom consistency. The Plexiglas tank and the phantom support were parallel to make the stress as uniaxial as possible. Moreover coupling gel was applied at the top and at the bottom of the phantoms to minimize friction effects between phantoms and supports.

Then, the 4.3 MHz ultrasonic array (128 elements, 0.33 mm pitch, 10 mm elevation, 60 mm elevation focus, Vermon, Tours, France) was applied at three different positions surrounding the phantoms as described on Fig. 1 to investigate the three possible shear wave propagations defined in part II. So, the ultrasonic beam was two times perpendicular [Figs. 1(a) and 1(c)] and one time parallel [Fig. 1(b)] to the uniaxial stress. The ultrasonic array was connected to an ultrafast scanner (the system was already describe in Ref. 31) and transmits ultrasound beams through a wide layer of coupling gel, which did not induce significant artifact on the applied uniaxial stress field.

To generate the radiation force, the ultrafast scanner was used to create an ultrasound-focused beam in the phantom at a chosen location (so called “supersonic push”). The typical ultrasound pulse was made of 500 oscillations at 4.3 MHz. This corresponded to a “pushing time” of $\sim 120 \mu\text{s}$. Just after the generation of the “pushing” beam, the scanner began an ultrafast imaging sequence by sending plane-wave insonifications at a high-frame rate (2000 Hz) in order to catch the shear wave created by the supersonic push.²²

In post acquisition, displacement fields were obtained by 1D cross correlation of beamformed RF signals stored with the reference echo image.³² The results were a set of images giving the displacement induced by the shear wave at each sample time (Fig. 3). In Fig. 3 one can also notice the effect of the attenuation on shear waves. Nevertheless, the attenuation is not relevant on the shear wave speed assessment because the signal to noise ratio is high enough to allow a good measurement of the displacements induced by shear waves along the imaged plane (about 25 mm, Fig. 3). The use of an inverse problem based on the Helmholtz equation, as described in previous papers,^{6,22} allowed us to map

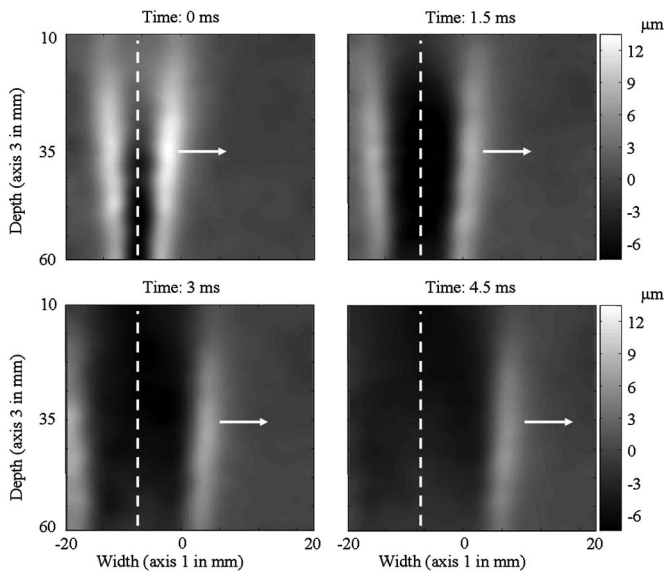


FIG. 3. Experimental displacement field in agar-gelatin phantom (GEL_1) at successive times after the “push”. The dotted line represents the axis of the polarization of the shear source (the supersonic push on axis 3) and the arrow the direction of propagation of the shear wave (axis 1).

the shear wave speed. Then knowing the density ($\rho_0 \approx 1000 \text{ kg/m}^3$), the shear modulus and its corresponding standard deviation, for each stress applied, were retrieved by taking the mean shear wave speed and its corresponding standard deviation at all depth between 0 and 20 mm in width (Fig. 4).

IV. RESULTS

The experiments on AG phantoms and on PVA phantoms were gathered in Figs. 5 and 6 respectively. Figures 5 and 6 showed an increasing speed versus applied stress for the shear wave propagating in the 13 plane and a decreasing speed in the 12 plane. The shear wave speed in the 21 plane was sometimes increasing and sometimes decreasing with respect to the applied stress, so it has an influence on both sign and value of the third order elastic coefficient (A). At the zero stress point for each data set, the shear Lamé coef-

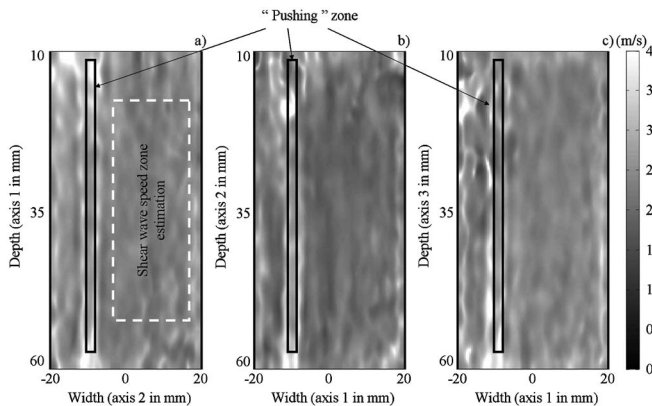


FIG. 4. Map of the shear wave speed for each position of the transducer array, (a) 12 (equivalent to 32), and (b) 21 (equivalent to 23), and (c) 31 (equivalent to 13) in AG phantom (GEL_1) at zero stress. The point line corresponds to the region of interest used for the estimation of the mean shear wave speed and its corresponding standard deviation.

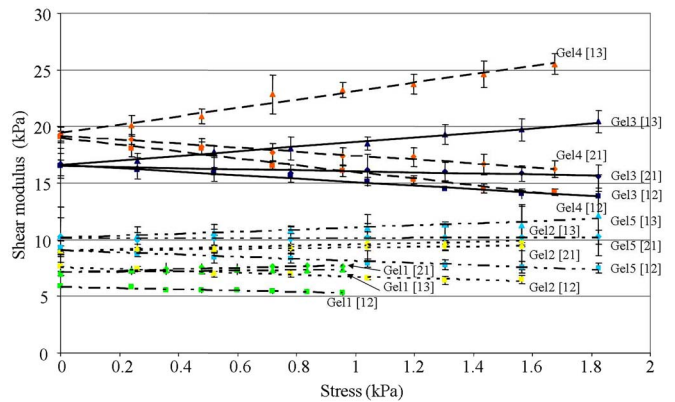


FIG. 5. (Color online) Experimental shear moduli as a function of applied uniaxial stress for each axis of propagation investigated in agar-gelatin phantoms. Four different phantoms with different gelatin concentration were investigated: Gel_1 (5% by weight of gelatin), Gel_2 (7%), Gel_3 (10%), Gel_4 (15%) and Gel_5 (8.5%). The slopes given by the dashed and solid lines were obtained from a least mean square fit.

ficient μ was computed as the mean value of the moduli measured for the three experimental configurations (Fig. 1). The values, summed up in Table I, show a good estimation of the linear shear modulus with a maximum 9% standard deviation in AG phantoms and 2% in PVA phantoms. As presented in Figs. 5 and 6, the shear modulus evolution clearly exhibits the appearance of an anisotropic behavior in all phantoms. Moreover, the shear modulus was linearly dependent with respect to the uniaxial stress in all materials as expected in the theoretical framework. From a quantitative point of view, the shear modulus affecting each quasi-plane shear wave (12, 21, 13) increased or decreased respectively with the following slopes (obtained from a least mean square fit of the data): GEL_1 (−0.56, 0.61, 0.26), GEL_2 (−0.79, 0.25, 0.59), GEL_3 (−1.55, −0.46, 2.03), GEL_4 (−3.02, −1.75, 3.71), GEL_5 (−0.94, 0.05, 0.92), PVA_1 (−0.48, 0.31, 0.55), PVA_2 (−1.11, −0.10, 1.26), and PVA_3 (−1.13, −0.23, 1.35). One can notice that when the linear shear modulus was higher, the value of slopes increased for the 13 plane and decreased for the 21 and 12 planes in both AG phantoms and PVA phantoms. Further, the slope for the

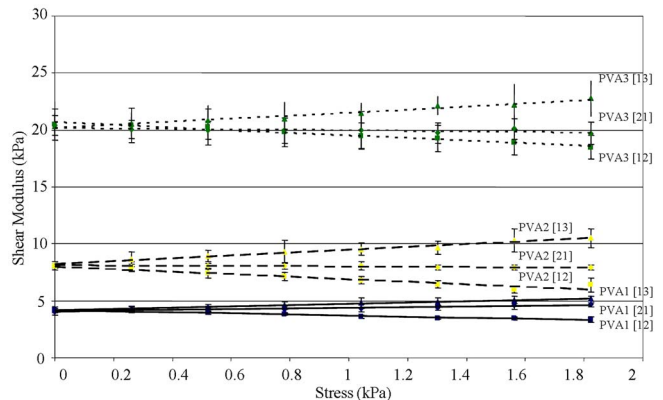


FIG. 6. (Color online) Experimental shear moduli as a function of applied uniaxial stress for each axis of propagation investigated in PVA phantoms. Three different phantoms, with different elasticity defined by the number of freezing-thawing cycles applied (2, 3, and 5 cycles), were investigated. The slopes given by the dashed and solid lines were obtained using a linear fit.

TABLE I. Elastic moduli measured in two different soft solids.

Materials	Linear shear modulus (Lamé coefficient μ (kPa) (mean value at 0 stress))	Non linear shear modulus [Landau coefficient A (kPa)]			
		Indice of propagation 12	Indice of propagation 21	Shear wave indices 13	Mean value
Agar-gelatin phantom 1	6.6±0.6	-35.0	-48.6	-29.4	-37.7±9.8
Agar-gelatin phantom 2	8.5±0.8	-21.5	-25.6	-21.0	-22.7±2.5
Agar-gelatin phantom 5	9.9±0.5	-7.1	-5.9	-4.8	-5.9±1.2
Agar-gelatin phantom 3	16.6±0.1	109.8	91.8	102.8	101.4±9.0
Agar-gelatin phantom 4	19.2±0.1	466.4	404.1	312.8	394.4±77.2
PVA phantom 1	4.1±0.1	-25.8	-15.4	-11.2	-17.5±7.5
PVA phantom 2	8.1±0.1	10.7	9.7	12.6	11.0±1.4
PVA phantom 3	20.4±0.1	31.8	56.3	42.8	43.6±12.2

[21](#) plane changed its sign with the stiffness of the material. In all experiments, correlation coefficients of estimated slopes using a linear fit were higher than 80% [except for two cases in AG phantoms (48% and 10%) and one case in PVA phantoms (51%)].

Using Eqs. [\(13\)–\(15\)](#), the experimental estimates of shear modulus versus axial stress slopes enable the calculation of the nonlinear Landau coefficient A for all soft solids. The mean value of A and its standard deviation were calculated from three independent values of A for each direction of propagation. One can notice that the standard deviation of A for all experiments in AG phantoms and PVA phantoms is less than 28% excluding for the one softer PVA phantom (43% in PVA_1).

Regarding the results presented in Table I, the nonlinear shear modulus A is plotted as a function of the shear modulus μ in Fig. 7. One can notice that A seems to evolve as an exponential as a function of μ for AG phantoms. For PVA phantoms, no specific variation can be observed.

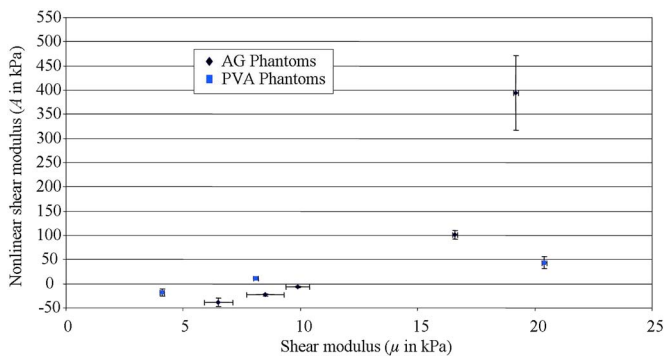


FIG. 7. (Color online) Experimental nonlinear shear moduli A as a function of experimental shear modulus μ for each phantom. In AG phantoms A seems to evolve as an exponential, but no specific variation can be noticed on PVA phantoms.

V. DISCUSSION

Results summarized in Table I confirm the fact that the experimental setup gives three independent ways to estimate the nonlinear coefficient A . Indeed, in the AG phantoms, estimates of A from the slopes obtained from shear wave velocities are in very good agreement for the four last phantoms (the standard deviation is less than 20%). AG phantom GEL_1 exhibits a 26% standard deviation for the A coefficient. In the PVA phantoms, the agreement for the different directions of propagation is also quite good: the standard deviation of the A coefficient estimates inferior to 28% for the two last phantoms. This can be explained by the difficulties to perfectly control the setup with such very soft phantoms, which cannot be submitted to large stresses in order to preserve their physical integrity, e.g., with a relatively large stress the phantoms are destroyed under the weight of the water tank. Nevertheless the same problem as in AG phantom appears for the very soft phantom PVA_1. Moreover, positioning the transducer array correctly with regards to the axis of the uniaxial stress is not trivial, since one cannot perfectly know the true spatial distribution of the uniaxial stress. However, compared to others results already reported in previous papers³³ for metals, crystals or polystyrene,³⁴ these experimental estimates of μ and A in soft solids confirm the fact that the A Landau coefficient exhibits values (kPa), consequently much lower than in classical solids.

Comparing results obtained in AG phantoms and in PVA phantoms, the shear modulus values are in the same range of elasticity for both type of phantoms. However, the behavior of the nonlinear coefficient A is quite different. For example, if one compares the AG phantom GEL_2 and the PVA phantom PVA_1, their shear moduli are practically the same (8.5±0.8 kPa and 8.15±0.1 kPa respectively). But the Landau coefficient A is negative in AG phantoms and positive in PVA phantoms. Moreover the range of elasticity of A is

TABLE II. Shear wave speed (13 direction) in an AG phantom (5% by weight of gelatin) at zero stress as a function of the height from the top of the phantom.

Shear modulus (kPa)	6.5±0.2	6.5±0.1	6.6±0.2	6.7±0.2	6.8±0.8
Height (cm)	2	4	6	8	10

larger in AG phantoms (from -37.7 to 394.4 kPa) than in PVA phantoms (from -17.5 to 43.6 kPa). Once again, comparing AG phantom GEL_4 and PVA phantom PVA_3, the shear modulus is quite identical but the A value is practically 10 times higher in AG phantom. Thus there is a big difference from the nonlinear point of view between these two kinds of material even though their linear behavior is quite similar.

The shear modulus at zero stress is determined by averaging the three measurements in each direction. On the one hand, the estimation of the shear modulus at zero stress in AG phantoms exhibits a quite small 7% standard deviation. The reason why the shear coefficient is not the same for all directions, as it should be in an ideally isotropic medium, is that the measurements were performed in the middle of the sample. For example, let us consider a horizontal plane at a given depth in the phantom with no uniaxial stress applied. Above this plane, the own weight of the phantom induces stress, which depends on the height of the column of the upper part of the material. Consequently, a uniaxial stress increasing with depth appears due to gravity effects. Thus, the speed of the shear waves measured should increase with depth. To confirm this argument, the shear wave speed was estimated at several depths within an AG phantom (GEL_1 with 5% by weight of gelatin and 3% of by weight of agar) from 2 cm top down to 10 cm with 2 cm steps. Resulting values for the 13 direction (the transducer array was horizontal) are summarized in Table II.

The shear wave speed increases as a function of the height and confirms the influence of the gravity force. Results presented on Fig. 5 show that this effect is much less pronounced as the gelatin concentration increases (and consequently shear modulus at zeros stress). On the other hand, in PVA phantoms the standard deviation also decreases to 2%. So, PVA phantoms seem to be less submitted to gravity effects. This is probably related to the internal structure of PVA phantoms³⁵ (polymer chains) more cross linked and stiffer compared to the internal structure of AG phantoms³⁶ (network of rigid gelatin rods). Nevertheless, these gravity effects do not affect drastically assessment of the third order elastic coefficient.

From Eqs. (13)–(15) one can see that starting from an isotropic solid the applied stress implies an anisotropic behavior of the material. In other words, modifying the stress is equivalent to induce an apparent anisotropy in the medium due to nonlinear effects. For a given stress one can define a specific nonlinear anisotropy corresponding to a specific set of different independent elastic constants (μ_{12} , μ_{21} , μ_{13}) depending of the nonlinear coefficient. At zero stress, velocities correspond to an isotropic solid ($\rho_0 V_{ij}^2 = \mu$; $i, j = 1, 2, 3$). It is

confirmed experimentally for PVA phantoms and the two stiffer AG phantoms, as all lines converge towards the same point at zero stress. However, for very soft solids, for example GEL_1, GEL_2, or GEL_5, an initial anisotropy was present due to gravity effects although the material was isotropic. Under their own weight net force, phantoms were naturally stressed and an apparent resulting anisotropy appears. In linear classical solids this kind of anisotropy was corresponding to a hexagonal system,²⁴ so called “transverse isotropy” because two shear waves speeds are identical in the plane defined by the polarization of the two waves; this plane can be defined as isotropic (The shear wave speeds assessed on the 21 and 13 direction were equivalent (GEL_1 (21 2.66 ± 0.06 m/s), 13 2.64 ± 0.03 m/s), GEL_2 (21 3.00 ± 0.08 m/s 13 3.00 ± 0.02 m/s), GEL_5 (21 3.20 ± 0.41 m/s, 13 3.21 ± 0.26 m/s)). Nevertheless, here the apparent anisotropy cannot be defined because anisotropy is defined with the symmetry of the second order elastic moduli. For instance the anisotropy induced by the stress effects must be distinguished from those caused by intrinsic material anisotropy.¹⁶ Now, for a higher uniaxial stress (e.g., $\sigma_{22} = 1.2$ kPa), in each material, three different velocities are observed (Figs. 5 and 6). One can notice that nonlinear effect increase the observed anisotropy and the behavior of the medium is more complicated. These experiments interestingly emphasize the fact that nonlinear effects significantly modify the anisotropic behavior of soft solids.

Moreover one can notice that when μ grows, A increases going from a negative value to a positive one for both AG phantoms and PVA phantoms. This is directly related to the slope variation of the shear wave speed along direction 21 which changes of sign, from positive to negative, as a function of the shear modulus increase. Consequently for certain shear modulus μ at zero stress, e.g., a certain concentration of agar-gelatin or a certain number of freezing–thawing cycles in PVA phantoms, the nonlinear shear modulus A is cancelled. Regarding Eqs. (13)–(15), anisotropy can be also retrieved if the nonlinear coefficient A is cancelled. In this specific configuration, the slope of the measurement for the couple of indices 21 [Eq. (14)] is null. The stress applied has no more effect on the shear wave velocity. But stress still induces anisotropy for both other couple of indices [Eqs. (13) and (15)]. Shear wave velocity in the 13 direction increases whereas shear wave velocity in 12 direction decreases with the applied stress. In fact, such an $A=0$ assumption means that the third invariant of the Lagrangian strain tensor I_3 has no effect in the development of the strain energy [Eq. (4)] (if one considers only the development of the strain energy at the third order). So, in that particular configuration, the only contribution to nonlinearity is the quadratic term from the strain tensor, also known as the geometric nonlinearity.

From Fig. 7, one can notice that the nonlinear parameter A seems to evolve as an exponential regarding to the shear modulus for the AG phantoms and it seems not to be the case for the PVA phantoms. These effects can be intuitively explained by the differences between microstructures of both materials. On the one hand, the elasticity results from the response of the polymeric filaments between cross-links,

from alterations in the network structure, or both.³⁷ On the other hand, the principles responsible for the nonlinear elasticity due to the microstructure are unknown, theories show that systems of filamentous proteins arranged in an open crosslinked mesh invariably stiffen at low strains without requiring specific architecture or multiple elements with different intrinsic stiffness.³⁸ Such behavior could be strongly interacting in such PVA phantoms known to contain crosslinked filaments. Moreover, as a comparison in classical solids such as glasses, the different constituent of the glasses used in the experiments can be related to velocity variations observed for both longitudinal and transversal waves in an acoustoelasticity experiments.^{39,40} However, the understanding of the behavior of the nonlinear shear modulus (A) as a function of the shear modulus (μ) needs further investigation.

VI. CONCLUSION

In this paper, a fast, simple, reproducible and robust method based on the supersonic shear imaging technique was used to revisit the acoustoelasticity experiment in order to characterize the nonlinear shear behavior of soft solids. This ultrasound-based technique enables both the remote generation in soft solids of quasiplane polarized shear waves and the ultrafast imaging of their resulting propagation. It enables the local assessment (or mapping) of the third order shear elastic coefficient A . Using an expression of the strain energy derived by Hamilton *et al.*²⁰ and Zabolotskaya *et al.*²¹ in quasiincompressible media, this third order coefficient can be estimated from a single ultrasonic experiment. Instead of measuring shear wave speeds for three different polarizations in order to completely determine the nonlinearity of standard solids, one single polarization experiment under a varying applied uniaxial stress is sufficient in soft solids to characterize the nonlinear shear elasticity. It means that *in vivo* assessment of this parameter could be feasible within the framework of the supersonic shear imaging approach.

ACKNOWLEDGMENTS

The authors would like to gratefully thank Patricia Daenens and Marc Yvert for technical assistance and Daniel Royer for illuminating discussion.

- ¹T. A. Krouskop, B. S. Dougherty, and F. S. Vinson, "A pulsed Doppler ultrasonic system for making noninvasive measurements of the mechanical properties of soft tissue," *J. Rehabil. Res. Dev.* **24**, 1–8 (1987).
- ²R. M. Lerner, K. J. Parker, J. Holen, R. Gramiak, and R. C. Waag, "Sonoelasticity: Medical elasticity images derives from ultrasound signals in mechanically vibrated targets," *Acoust. Imaging* **16**, 317–327 (1988).
- ³Y. Yamakoshi, J. Sato, and T. Sato, "Ultrasonic imagins of internal vibration of soft tissue under forced vibration," *IEEE Trans. Ultrason. Ferroelectr. Freq. Control* **37**, 45–53 (1990).
- ⁴K. J. Parker and R. M. Lerner, "Sonoelasticity of organs: Shearwaves ring a bell," *J. Ultrasound Med.* **11**, 387–392 (1992).
- ⁵S. F. Levinson, M. Shinagawa, and T. Sato, "Sonoelastic determination of human skeletal muscle elasticity," *J. Biomech.* **28**, 1145–1154 (1995).
- ⁶J. Bercoff, S. Chaffai, M. Tanter, L. Sandrin, S. Catheline, M. Fink, J.-L. Gennisson, and M. Meunier, "*In vivo* breast tumor detection using transient elastography," *Ultrasound Med. Biol.* **29**, 1387–1396 (2003).
- ⁷L. Sandrin, B. Fourquet, J.-M. Hasquenoph, S. Yon, C. Fournier, F. Mal, C. Christidis, M. Ziol, B. Poulet, F. Kazemi, M. Beauprand, and R. Palau, "Transient elastography: a new non invasive method for assessment of

- hepatic fibrosis," *Ultrasound Med. Biol.* **29**, 1705–1713 (2003).
- ⁸J.-L. Gennisson, S. Catheline, and M. Fink, "Transient elastography in anisotropic medium: application to the measurement of slow and fast shear wave speeds in muscles," *J. Acoust. Soc. Am.* **114**, 536–541 (2003).
- ⁹S. Catheline, J.-L. Gennisson, G. Delon, R. Sinkus, M. Fink, S. Abouelkaram, and J. Culioli, "Measurement of viscoelastic properties of homogeneous soft solid using transient elastography: An inverse problem approach," *J. Acoust. Soc. Am.* **116**, 3734–3741 (2004).
- ¹⁰J. Bercoff, M. Tanter, M. Muller, and M. Fink, "The role of viscosity in the impulse diffraction field of elastic waves induced by the acoustic radiation force," *IEEE Trans. Ultrason. Ferroelectr. Freq. Control* **51**, 1523–1536 (2004).
- ¹¹S. Catheline, J.-L. Gennisson, and M. Fink, "Measurement of elastic nonlinearity of soft solids with transient elastography," *J. Acoust. Soc. Am.* **114**, 3087–3091 (2003).
- ¹²S. Catheline, J.-L. Gennisson, M. Tanter, and M. Fink, "Observation of shock transverse waves in elastic media," *Phys. Rev. Lett.* **91**, 43011–43014 (2003).
- ¹³X. Jacob, J.-L. Gennisson, S. Catheline, M. Tanter, C. Barrière, D. Royer, and M. Fink, "Study of elastic nonlinearity of soft solids with transient elastography," *Proc.-IEEE Ultrason. Symp.* **1**, 660–663 (2003).
- ¹⁴D. S. Hugues and J. L. Kelly, "Second-order elastic deformation of solids," *Phys. Rev.* **92**, 1145–1149 (1953).
- ¹⁵T. D. Murnaghan, *Finite Deformation of an Elastic Solid* (Wiley, New York, 1951).
- ¹⁶A. Norris, *Non Linear Acoustics: Finite Amplitude Waves in Solids*, edited by M. Hamilton (Academic, New York, 1998).
- ¹⁷H. Kobayashi and R. Vanderby, "New strain energy function for acoustoelasticity analysis of dilatational waves in nearly incompressible hyperelastic materials," *J. Appl. Mech.* **72**, 843–851 (2005).
- ¹⁸H. Kobayashi and R. Vanderby, "Acoustoelastic analysis of reflected waves in nearly incompressible, hyper-elastic materials: Forward and inverse problem," *J. Acoust. Soc. Am.* **121**, 879–887 (2007).
- ¹⁹R. Q. Erkamp, A. R. Skovoroda, S. Y. Emelianov, and M. O'Donnell, "Measuring the nonlinear elastic properties of tissue-like phantoms," *IEEE Trans. Ultrason. Ferroelectr. Freq. Control* **51**, 410–419 (2004).
- ²⁰M. F. Hamilton, Y. A. Ilinskii, and E. A. Zabolotskaya, "Separation of compressibility and shear deformation in the elastic energy density (L)," *J. Acoust. Soc. Am.* **116**, 41–44 (2004).
- ²¹E. A. Zabolotskaya, M. F. Hamilton, Y. A. Ilinskii, and G. D. Meegan, "Modeling of non linear shear waves in soft solids," *J. Acoust. Soc. Am.* **116**, 2807–2813 (2004).
- ²²J. Bercoff, M. Tanter, and M. Fink, "Supersonic shear imaging: a new technique for soft tissues elasticity mapping," *IEEE Trans. Ultrason. Ferroelectr. Freq. Control* **51**, 374–409 (2004).
- ²³L. D. Landau and E. M. Lifshitz, *Theory of Elasticity*, 3rd ed. (Butterworth-Heinemann, Oxford, 2002).
- ²⁴D. Royer and E. Dieulesaint, *Elastic Waves in Solid* (Springer, Berlin, 1996), Vol. 1.
- ²⁵P. A. Johnson and P. Rasolofosaon, "Nonlinear elasticity and stress-induced anisotropy in rock," *J. Geophys. Res.* **101**, 3113–3124 (1995).
- ²⁶S. Kostek, B. K. Sinha, and A. N. Norris, "Third-order elastic constants for an inviscid fluid," *J. Acoust. Soc. Am.* **94**, 3014–3017 (1993).
- ²⁷R. N. Thurston and K. Brugger, "Third-order elastic constants and the velocity of small amplitude elastic waves in homogeneously stressed media," *Phys. Rev.* **133**, A1604–A1610 (1964).
- ²⁸J.-L. Gennisson and G. Cloutier, "Sol-gel transition in agar-gelatin mixtures studied with transient elastography," *IEEE Trans. Ultrason. Ferroelectr. Freq. Control* **53**, 716–723 (2006).
- ²⁹J. Fromageau, E. Brusseau, D. Vray, G. Gimenez, and P. Delachartre, "Characterization of PVA cryogel for intravascular ultrasound elasticity imaging," *IEEE Trans. Ultrason. Ferroelectr. Freq. Control* **50**, 1318–1324 (2003).
- ³⁰J. Fromageau, J.-L. Gennisson, C. Schmitt, R. Maurice, R. Mongrain, and G. Cloutier, "Estimation of polyvinyl alcohol cryogel mechanical properties with 4 ultrasound elastography methods and comparison with gold standard testings," *IEEE Trans. Ultrason. Ferroelectr. Freq. Control* **54**, 498–509 (2007).
- ³¹L. Sandrin, M. Tanter, S. Catheline, and M. Fink, "Shear modulus imaging using 2d transient elastography," *IEEE Trans. Ultrason. Ferroelectr. Freq. Control* **49**, 426–435 (2002).
- ³²J. Ophir, I. Céspedes, H. Ponnekanti, Y. Yasdi, and X. Li, "Elastography: a quantitative method for imaging the elasticity of biological soft tissues," *Ultrason. Imaging* **13**, 111–134 (1991).

- ³³M. A. Breazeale, "Comparison of the non linear behavior of fluids and solids," *Proceedings of the 13th ISNA*, World Scientific, Singapore, 1993, p. 451.
- ³⁴K. Naugolnykh and L. Ostrovsky, *Nonlinear Wave Processes in Acoustics* (Cambridge University Press, New York, 1998), Chap. 1, pp. 15–16.
- ³⁵C. M. Hassan and N. A. Peppas, "Structure and applications of polyvinyl alcohol hydrogels produced by conventional crosslinking or by freezing/thawing methods," *Adv. Polym. Sci.* **153**, 37–65 (2000).
- ³⁶C. Joly-Duhamel, D. Hellio, A. Ajdari, and M. Djabourov, "All gelatin networks: 2. The master curve for elasticity," *Langmuir* **18**, 7158–7166 (2002).
- ³⁷P. R. Onck, T. Koeman, T. van Dillen, and E. vander Giessen, "Alternative explanation of stiffening in cross-linked semiflexible networks," *Phys. Rev. Lett.* **95**, 178102 (2005).
- ³⁸C. Storm, J. J. Pastore, F. C. MacKintosh, T. C. Lubensky, and P. A. Janmey, "Nonlinear elasticity in biological gels," *Nature (London)* **435**, 191–194 (2005).
- ³⁹R. J. Wang, W. H. Wang, F. Y. Li, L. M. Wang, Y. Zhang, P. Wen, and J. F. Wang, "The Gruneisen parameter for bulk amorphous materials," *J. Phys.: Condens. Matter* **15**, 603–608 (2003).
- ⁴⁰B. Zhang, R. J. Wang, and W. H. Wang, "Response of acoustic and elastic properties to pressure and crystallization of Ce-based bulk metallic glass," *Phys. Rev. B* **72**, 104205 (2005).